Table 1. GRNs built in this study.

Network type	Study	Note	N	Network label
Tissue	Stelpflug et al. 2016	B73	93	Stelpflug2016 B73 [93]
	Walley et al. 2016	B73	23	Walley2016 B73 [23]
	Zhou et al. 2018	B73	23	Zhou2018 B73 [23]
		Mo17	23	Zhou2018 Mo17 [23]
		BxM	23	Zhou2018 BxM [23]
	Yi et al. 2019	seed dev	31	Yi2019 seed dev [31]
	Tissue Atlas	combined	247	Tissue Atlas combined [247]
Genotype	Eichten et al. 2013	seedling_leaf3	62	Eichten2013 seedling_leaf3 [62]
	Fu et al. 2013	kernel	368	Fu2013 kernel [368]
	Hirsch et al. 2014	seedling	503	Hirsch2014 seedling [503]
	Leiboff et al. 2015	SAM	383	Leiboff2015 SAM [383]
	Lin et al. 2017	ear	26	Lin2017 ear [26]
		root	27	Lin2017 root [27]
		shoot	27	Lin2017 shoot [27]
		tassel	26	Lin2017 tassel [26]
		SAM	27	Lin2017 SAM [27]
	Kremling et al. 2018	GRoot	201	Kremling2018 GRoot [201]
		GShoot	271	Kremling2018 GShoot [271]
		Kern	226	Kremling2018 Kern [226]
		L3Base	254	Kremling2018 L3Base [254]
		L3Tip	257	Kremling2018 L3Tip [257]
		LMAD	199	Kremling2018 LMAD [199]
		LMAN	249	Kremling2018 LMAN [249]
	Shaefer et al. 2018	root_GCN	48	Shaefer2018 root_GCN [48]
	Huang et al. 2018	leaf	394	Huang2018 leaf [394]
		root	176	Huang2018 root [176]
		SAM	406	Huang2018 SAM [406]
		seed	159	Huang2018 seed [159]
	Mazaheri et al. 2019	seedling	453	Mazaheri2019 seedling [453]
	Li et al. 2019	endosperm	121	Li2019 endosperm [121]
		internode	77	Li2019 internode [77]
		leaf	84	Li2019 leaf [84]
		root	84	Li2019 root [84]
		shoot	85	Li2019 shoot [85]
		seedling	169	Li2019 seedling [169]
Tissue*Genotype	Lin et al. 2017	5 tissues	133	Lin2017 5 tissues [133]
	Kremling et al. 2018	7 tissues	1,657	Kremling2018 7 tissues [1657]
	Huang et al. 2018	4 tissues	1,136	Huang2018 4 tissues [1136]
	Zhou et al. 2018	B+M+F1	73	Zhou2018 B+M+F1 [73]
	Li et al. 2019	6 tissues	620	Li2019 6 tissues [620]
RIL	Li et al. 2013	B73 x Mo17	107	Li2013 B73 x Mo17 [107]
	Baute et al. 2016	MAGIC	102	Baute2016 MAGIC [102]
	Baute et al. 2015	B73 x H99	106	Baute2015 B73 x H99 [106]
	Wang et al. 2018	W22 x Teosinte	617	Wang2018 W22 x Teosinte [617]

Table S1. TF knockout mutant RNA-Seq datasets used in this study.

TF alias	TF name	TF ID	Study	Accession	Tissue	N
kn1	knotted1	Zm00001d033859	Bolduc2012	PRJNA168086	meristem	10
cle7	clavata3/esr-related7	GRMZM2G372364		PRJNA494874	ear tip	4
rbm48	RNA binding motif protein 48	Zm00001d054077		PRJNA485828	endosperm	16
dek42	RNA binding motif protein 48	Zm00001d054077		PRJNA485820	kernel	6
mads47	MADS-transcription factor 47	Zm00001d046053		PRJNA289143	kernel	2
ufo1	unstable factor for orange1	Zm00001d000009	Wittmeyer2018	PRJNA483200	pericarp	27
rel2	ramosa1 enhancer locus2	Zm00001d024523	Liu2018	PRJNA475209	tassel	6
o2	opaque2	Zm00001d018971	Zhan2018	PRJNA471036	endosperm	6
o2_b	opaque2	Zm00001d018971	Li2015	PRJNA262503	endosperm	2
bzip22	bZIP-transcription factor 22	Zm00001d021191	Li2018	PRJNA449867	kernel	6
fl3	floury3	Zm00001d009292	Li2017	PRJNA375801	endosperm	6
fea4	fasciated ear4	Zm00001d037317	Pautler2015	PRJNA262781	ear primordia	6
liguleless	liguleless1	Zm00001d002005	Johnston2014	PRJNA260793	leaf primordia	24
nkd	naked endosperm1	Zm00001d002654	Gontarek2016	PRJNA260183	aleurone, endosperm	2
sk1	silkless ears1	Zm00001d002970		PRJNA483310	young V9 tassel	6
dek15	defective kernel15	Zm00001d052197		PRJNA494076	kernel	6
ra1	RAMOSA1	Zm00001d020430	Eveland2014	PRJNA219746	ear	10
ra2	RAMOSA2	Zm00001d039694	Eveland2014	PRJNA219746	ear	10
ra3	RAMOSA3	Zm00001d022193	Eveland2014	PRJNA219746	ear	10
P1	Pericarp Color1	Zm00001d028842	Morohashi2012	PRJNA167802	pericarp	6
hda101	RPD3 histone deacetylase homolog	Zm00001d053595	Yang2016	PRJNA305809	seed	6

Table S2. Natural variation datasets used for validation in this study.

author	study	condition	contrast	non-DE	DE1-2	DE2-4	DE4+	SPE
Waters2017	stress cis-trans	leaf3 cold	B73 vs B37	14,991	5,508	2,524	2,191	765
		leaf3 cold	B73 vs Oh43	13,985	6,013	2,955	2,226	800
		leaf3 control	B73 vs B37	11,868	7,131	3,468	2,551	961
		leaf3 control	B73 vs Oh43	12,804	6,395	3,213	2,545	1,022
		leaf3 heat	B73 vs B37	14,488	5,491	2,937	2,276	787
		leaf3 heat	B73 vs Oh43	13,304	5,931	3,249	2,568	927
		leaf3 cold	B73 vs Mo17	17,235	2,783	2,136	1,550	796
		leaf3 cold	B73 vs PH207	17,202	3,023	2,075	1,439	761
		leaf3 control	B73 vs Mo17	18,843	2,012	1,610	1,226	809
		leaf3 control	B73 vs PH207	19,148	1,868	1,447	1,239	798
		leaf3 heat	B73 vs Mo17	18,453	2,433	1,641	1,152	821
		leaf3 heat	B73 vs PH207	16,533	3,404	2,312	1,459	792
Marcon2017	drought stress	root control	B73 vs Mo17	13,185	6,718	2,513	1,940	651
		root drought	B73 vs Mo17	13,828	6,370	2,347	1,864	598
Sun2018	mo17 genome	bract	B73 vs Mo17	19,008	832	980	1,192	702
		endosperm	B73 vs Mo17	18,841	1,021	1,240	1,016	596
		root	B73 vs Mo17	18,760	820	1,114	1,371	649
		seedling	B73 vs Mo17	19,416	661	850	980	807
		stem	B73 vs Mo17	18,669	887	1,130	1,164	864
Zhou2018	B73 Mo17 atlas	auricle	B73 vs Mo17	14,944	3,885	2,596	2,091	860
		blade leaf	B73 vs Mo17	16,331	3,174	2,170	1,775	926
		coleoptile	B73 vs Mo17	18,653	2,392	1,389	1,367	575
		ear	B73 vs Mo17	18,838	2,425	1,213	1,095	805
		embryo	B73 vs Mo17	16,351	3,577	2,227	1,407	814
		endosperm14D	B73 vs Mo17	17,848	2,570	1,748	1,468	742
		endosperm27D	B73 vs Mo17	16,695	3,105	2,254	1,458	864
		flag leaf	B73 vs Mo17	16,090	3,146	2,329	1,898	913
		floret	B73 vs Mo17	17,037	3,259	1,977	1,342	761
		husk	B73 vs Mo17	16,723	3,362	1,809	1,605	877
		internode	B73 vs Mo17	13,644	4,273	2,844	2,653	962
		kernel	B73 vs Mo17	17,590	2,946	1,734	1,362	744
		radicle root	B73 vs Mo17	18,120	2,346	1,764	1,501	645
		root	B73 vs Mo17	17,334	2,883	1,844	1,499	816
		seed imbibed	B73 vs Mo17	12,068	5,342	3,606	2,626	734
		seedling leaf	B73 vs Mo17	16,245	2,938	2,286	2,079	828
		seedling meristem	B73 vs Mo17	19,207	1,923	1,249	1,235	762
		seedling root	B73 vs Mo17	18,842	2,009	1,631	1,180	714
		sheath	B73 vs Mo17	15,209	3,885	2,633	1,810	839
		silk	B73 vs Mo17	15,378	3,577	2,303	2,152	966
		spikelet	B73 vs Mo17	17,984	2,736	1,589	1,209	858
		tassel	B73 vs Mo17	15,594	3,856	2,435	1,677	814
		tassel stem	B73 vs Mo17	12,564	4,625	3,512	2,652	1,023

Table S3. GRN-predicted TFs supported by trans-eQTL hotspots.

ID	Support eQTL study	Support GRN	TF Annotation	Target enrichment
Zm00001d001945	li2013,li2013,wang201	fu2013, leiboff2015, lin2017, li2019, wang2018, huang2018, zhou2018, li2013, baute2015	Auxin response factor 4	(25) histone H3-K9 methylation; (9) cytokinesis by cell plate formation; (8) cell proliferation
Zm00001d003162	li2013,li2013	tissue atlas, leiboff2015, mazaheri2019, huang2018, li2013, kremling2018, zhou2018, baute2016, baute2015	Zinc finger protein CONSTANS-LIKE 5	(57) cysteine biosynthetic process; (45) photosynthesis, light harvesting in photosystem I; (38) photosynthesis light reactions; (16) rRNA processing; (15) photosystem II assembly; (8) Calvin-Benson-Bassham cycle
Zm00001d003195	li2013	tissue atlas, zhou2018	Salt tolerance-like protein	(9) rRNA processing; (8) Calvin-Benson-Bassham cycle
Zm00001d004095	wang2018	li2013, baute2016	basic helix-loop-helix (bHLH) DNA-binding superfamily protein	
Zm00001d004358	wang2018	baute2016, wang2018		(11) pentose-phosphate shunt
Zm00001d004497	liu2017,wang2018	baute2015, wang2018, baute2016, baute2015, wang2018	C2H2-like zinc finger protein	
Zm00001d005016	liu2017,wang2018	baute2016, baute2015, baute2016, baute2015	WRI1 transcription factor1	(22) glycolysis I (from glucose 6-phosphate)
Zm00001d006578	li2013	li2013, baute2015	Transcription factor bHLH130	(11) L-alanine degradation II (to D-lactate)
Zm00001d006701	li2013	li2013, baute2015	GRAS transcription factor	(6) C4 photosynthetic carbon assimilation cycle, PEPCK type
Zm00001d006721	li2013	li2013, baute2015	Protein SHORT-ROOT	
Zm00001d010060	liu2017	baute2015, wang2018	BEL1-like homeodomain protein 9	
Zm00001d010785	liu2017	li2013, baute2015	Putative GATA transcription factor family protein	
Zm00001d012544	wang2018	li2013, baute2015	myb domain protein 81	(6) glycolysis I (from glucose 6-phosphate)
Zm00001d012605	wang2018	li2013, baute2015	MRP interacting1	
Zm00001d013547	li2013	li2013, baute2015	BEL1-like homeodomain protein 3	
Zm00001d015412	wang2018	li2013, baute2015	sequence-specific DNA binding transcription factors	(10) suberin monomers biosynthesis
Zm00001d017788	wang2018	li2013, baute2016, baute2015	Dof zinc finger protein DOF2.1	
Zm00001d017900	wang2018	li2013, wang2018	Dof zinc finger protein DOF5.4	
Zm00001d018225	wang2018	li2013, baute2016	Homeodomain leucine zipper family IV protein	(27) triacylglycerol degradation; (15) phenylpropanoid biosynthesis; (11) very long chain fatty acid biosynthesis I
Zm00001d018465	wang2018	li2013, baute2016, baute2015		

Zm00001d020019	liu2017	li2013, baute2016, baute2015	Protein PHR1-LIKE 3	
Zm00001d020043	liu2017,wang2018	li2013, baute2016, baute2015, li2013, baute2015	Ethylene-responsive transcription factor ERF117	
Zm00001d020408	wang2018	li2013, baute2015	Typical P-type R2R3 Myb protein	
Zm00001d021403	wang2018	li2013, baute2015	indeterminate1 domain7	(9) UDP-sugars interconversion
Zm00001d021442	wang2018	mazaheri2019, baute2015	Protein NLP2	(6) sucrose degradation II (sucrose synthase)
Zm00001d021701	wang2018	li2013, wang2018	Transcription factor ILR3	
Zm00001d024041	liu2017	li2013, baute2015	bZIP transcription factor 16	
Zm00001d024230	liu2017,wang2018	li2013, baute2015, li2013, baute2015	Nuclear transcription factor Y subunit C-2	
Zm00001d024268	wang2018	li2013, baute2015	NAC domain-containing protein 21/22	
Zm00001d024323	wang2018	eichten2013, baute2015	Putative WRKY DNA-binding domain superfamily protein	(48) flavonoid biosynthesis (in equisetum); (16) anthocyanin biosynthesis
Zm00001d026147	wang2018	eichten2013, li2013, baute2015	plant color component at R1	(14) L-glutamine degradation I; (12) anthocyanin biosynthesis; (11) glycerophosphodiester degradation; (10) flavonoid biosynthesis (in equisetum)
Zm00001d026271	wang2018	li2013, baute2015	Putative AP2/EREBP transcription factor superfamily protein	
Zm00001d026448	wang2018	li2013, baute2015	Floral homeotic protein APETALA 2	(11) proanthocyanidins biosynthesis from flavanols
Zm00001d028007	wang2018	baute2016, baute2015	Calmodulin-binding transcription activator 2	(26) gluconeogenesis I; (7) fatty acid biosynthesis initiation I
Zm00001d029934	wang2018	li2013, baute2015	Homeobox-leucine zipper protein HAT4	
Zm00001d029963	wang2018	baute2015, wang2018	myb-like transcription factor family protein	
Zm00001d030028	li2013,wang2018	leiboff2015, huang2018, li2013, baute2016, baute2015, li2013, baute2016	myc transcription factor7	(48) response to wounding; (15) cutin biosynthesis; (10) regulation of transcription, DNA-templated; (8) jasmonic acid biosynthesis; (6) regulation of transcription, DNA-templated; (5) response to wounding
Zm00001d030727	wang2018	li2013, baute2015	Dof zinc finger protein DOF2.2	(11) cell proliferation; (9) regulation of transcription, DNA-templated
Zm00001d030907	wang2018	li2013, baute2015	B3 domain-containing protein	
Zm00001d030908	wang2018	li2013, baute2015	B3 domain-containing protein	
Zm00001d031561	wang2018	baute2015, wang2018	Transcription factor bHLH62	(24) response to wounding; (7) response to wounding
Zm00001d031665	wang2018	baute2016, baute2015	Transcription factor bHLH137	(12) triacylglycerol degradation

Zm00001d033898	li2013,li2013,wang201	tissue atlas, lin2017, li2019, zhou2018, kremling2018, huang2018, baute2016, baute2015, tissue atlas, huang2018	BEL1-like homeodomain protein 4	(34) Calvin-Benson-Bassham cycle; (23) photosystem II assembly; (10) rRNA processing; (9) isopentenyl diphosphate biosynthetic process, methylerythritol 4-phosphate pathway; (7) gluconeogenesis I; (7) photosynthesis light reactions; (7) response to cytokinin; (7) positive regulation of transcription, DNA-templated; (6) photosynthetic electron transport in photosystem I; (5) response to salt stress
Zm00001d034984	li2013	tissue atlas, zhou2018	Putative NAC domain transcription factor superfamily protein	
Zm00001d035084	li2013,li2013	shaefer2018, baute2015, li2013, baute2016	Putative NAC domain transcription factor superfamily protein	
Zm00001d035195	li2013	tissue atlas, huang2018	Protein LSD1	(6) GDP-mannose biosynthesis
Zm00001d035224	liu2017	lin2017, zhou2018	protein	
Zm00001d036214	li2013	li2013, baute2016	B-box zinc finger protein 22	(20) glycolysis I (from glucose 6-phosphate)
Zm00001d036364	wang2018	eichten2013, kremling2018, wang2018	NAC domain containing protein 36	(8) glycerophosphodiester degradation
Zm00001d041831	liu2017	baute2016, baute2015	DNA binding protein	
Zm00001d042463	li2013	huang2018, li2013	Two-component response regulator ARR11	
Zm00001d043420	li2013,li2013,li2013	kremling2018, baute2016, shaefer2018, li2019, tissue atlas, lin2017, zhou2018, li2013	Basic leucine zipper 34	(20) homogalacturonan degradation
Zm00001d044260	li2013,wang2018	li2013, baute2015, li2013, baute2015	C3H-type transcription factor	
Zm00001d044355	wang2018	li2013, baute2015	B3 domain-containing protein	
Zm00001d044538	li2013	huang2018, zhou2018		(8) regulation of transcription by RNA polymerase II; (7) cellulose biosynthesis; (7) triacylglycerol degradation
Zm00001d045581	liu2017	li2013, baute2016, baute2015	Putative MYB DNA-binding domain superfamily protein	
Zm00001d045661	li2013,liu2017,wang20	tissue atlas, eichten2013, mazaheri2019, lin2017, kremling2018, huang2018, li2019, zhou2018, li2013, baute2015, tissue atlas, huang2018	Zinc finger protein CONSTANS-LIKE 16	(66) rRNA processing; (21) photosynthesis light reactions; (14) photosynthesis, light harvesting in photosystem I; (12) thylakoid membrane organization; (12) RNA modification; (10) response to cytokinin; (7) Calvin-Benson-Bassham cycle; (6) chloroplast organization
Zm00001d046323	liu2017	fu2013, li2013, baute2016, baute2015		

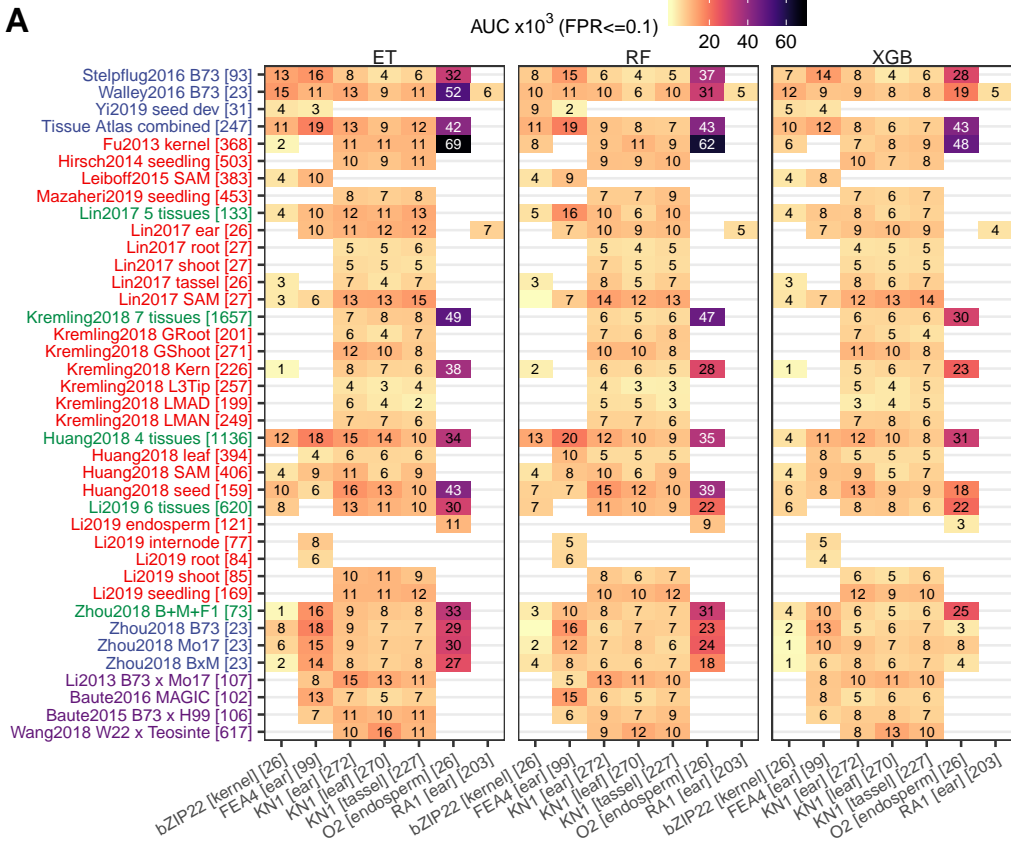|				
Zm00001d046405	li2013,liu2017,liu2017	tissue atlas, eichten2013, lin2017, kremling2018, huang2018, li2019, zhou2018, baute2016, wang2018, leiboff2015, shaefer2018, li2013, baute2015, tissue atlas, huang2018	Putative homeodomain-like transcription factor superfamily protein	(89) isopentenyl diphosphate biosynthetic process, methylerythritol 4-phosphate pathway; (60) thylakoid membrane organization; (24) 3,8-divinyl-chlorophyllide *a* biosynthesis I (aerobic, light-dependent); (18) positive regulation of transcription, DNA-templated; (13) pyrimidine ribonucleotides interconversion; (12) RNA modification; (10) chloroplast organization; (10) palmitate biosynthesis II (bacteria and plants); (6) chloroplast organization; (6) tetrapyrrole biosynthesis I (from glutamate)
Zm00001d046441	liu2017	li2013, baute2016, baute2015	FAR1-domain family sequence	(7) formate oxidation to CO_2
Zm00001d047519	li2013,wang2018	leiboff2015, shaefer2018, lin2017, li2013, baute2015	basic leucine-zipper 52	(15) cell proliferation
Zm00001d047563	wang2018	li2013, baute2015	ethylene insensitive-like1	(6) translation
Zm00001d047968	wang2018	li2013, baute2015	Zinc finger protein 1	
Zm00001d047999	wang2018	li2013, baute2015	Putative HLH DNA-binding domain superfamily protein	
Zm00001d051573	li2013	leiboff2015, lin2017, zhou2018	Putative homeobox DNA-binding domain superfamily protein	
Zm00001d052798	li2013	leiboff2015, shaefer2018, li2013	Homeodomain-like superfamily protein	
Zm00001d052847	wang2018	li2013, baute2016, baute2015	Putative WRKY DNA-binding domain superfamily protein	
Zm00001d053124	li2013	tissue atlas, kremling2018, huang2018, li2019, zhou2018	myb domain protein 60	(33) thylakoid membrane organization; (30) isopentenyl diphosphate biosynthetic process, methylerythritol 4-phosphate pathway; (22) rRNA processing; (17) triacylglycerol degradation; (11) response to cold; (9) chloroplast organization; (7) photosystem II assembly; (7) Calvin-Benson-Bassham cycle; (5) photosynthesis light reactions; (5) RNA modification
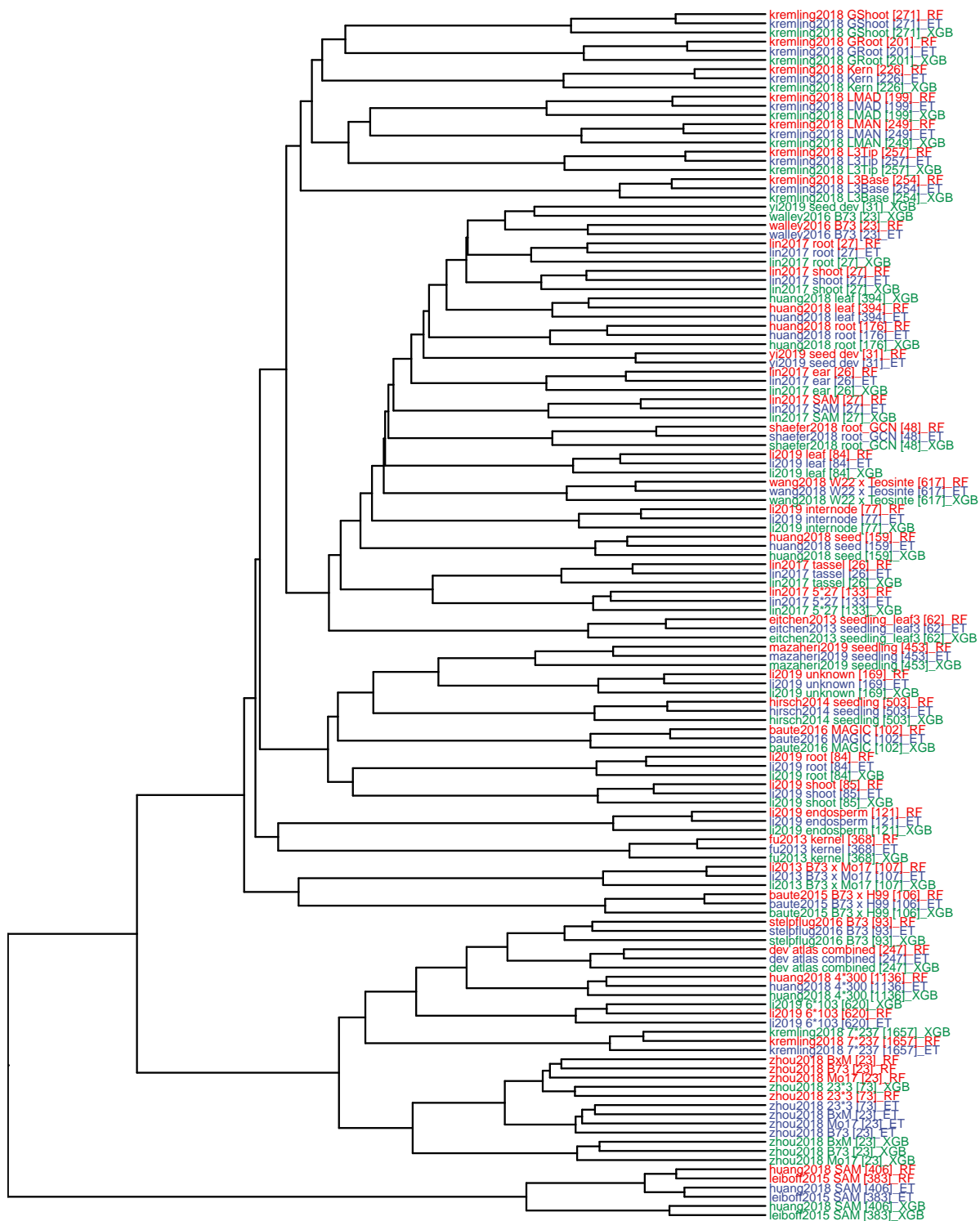
Figure S1. Hierarchical clustering of 132 GRNs (44 expression dataset * 3 methods). Each of the three regression-based method (random forest, extra trees, gradient boosted) was used to build a network for each RNA-Seq dataset. Pairwise distance between networks was determined by taking the top 100,000 TF-target predictions from each network and calculating the proportion of shared (common) predictions (using 'dist()'

function in R with additional argument 'method=binary'). Hierarchical clustering was then performed based on the cross-network pairwise distance matrix using "ward.D" option.
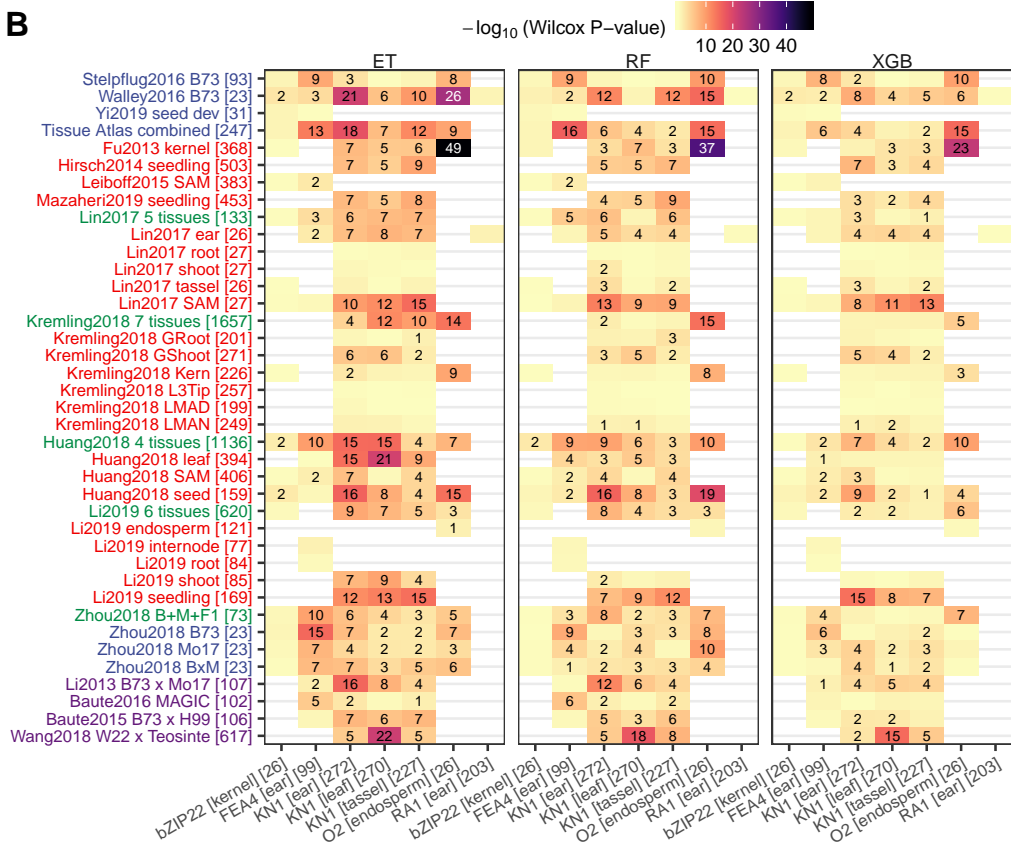
Figure S2a. Comparison of GRNs built with different methods using supports from known direct targets of published TF studies in maize.

Figure S2b. Comparison of GRNs built with different methods using supports from TF knockout mutant RNA-Seq data.

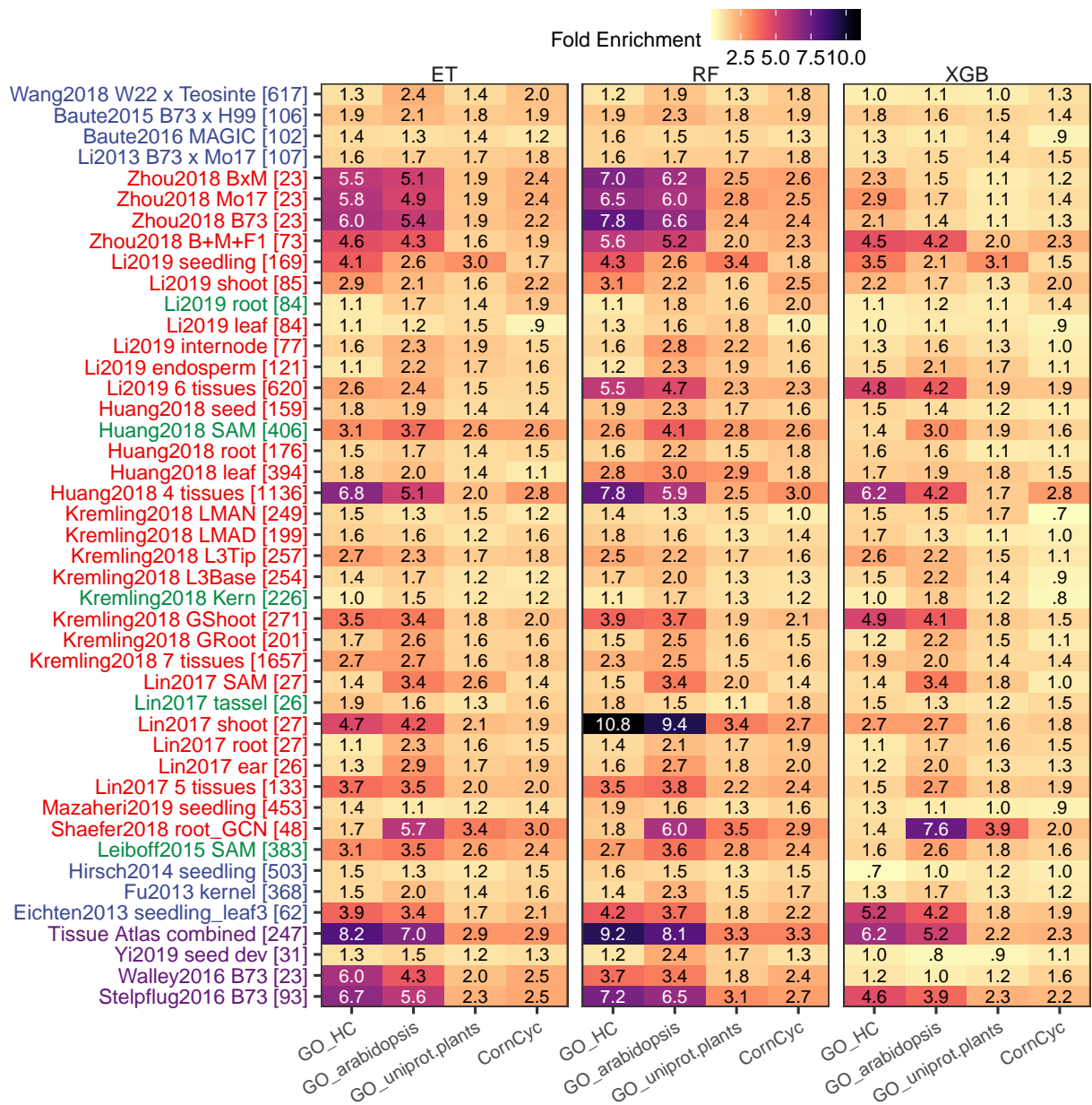| Dataset	ET GO_HC	ET GO_arabidopsis	ET GO_uniprot.plants	ET CornCyc	RF GO_HC	RF GO_arabidopsis	RF GO_uniprot.plants	RF CornCyc	XGB GO_HC	XGB GO_arabidopsis	XGB GO_uniprot.plants	XGB CornCyc
Wang2018 W22 x Teosinte [617]	1.3	2.4	1.4	2.0	1.2	1.9	1.3	1.8	1.0	1.1	1.0	1.3
Baute2015 B73 x H99 [106]	1.9	2.1	1.8	1.9	1.9	2.3	1.8	1.9	1.8	1.6	1.5	1.4
Baute2016 MAGIC [102]	1.4	1.3	1.4	1.2	1.6	1.5	1.5	1.3	1.3	1.1	1.4	.9
Li2013 B73 x Mo17 [107]	1.6	1.7	1.7	1.8	1.6	1.7	1.7	1.8	1.3	1.5	1.4	1.5
Zhou2018 BxM [23]	5.5	5.1	1.9	2.4	7.0	6.2	2.5	2.6	2.3	1.5	1.1	1.2
Zhou2018 Mo17 [23]	5.8	4.9	1.9	2.4	6.5	6.0	2.8	2.5	2.9	1.7	1.1	1.4
Zhou2018 B73 [23]	6.0	5.4	1.9	2.2	7.8	6.6	2.4	2.4	2.1	1.4	1.1	1.3
Zhou2018 B+M+F1 [73]	4.6	4.3	1.6	1.9	5.6	5.2	2.0	2.3	4.5	4.2	2.0	2.3
Li2019 seedling [169]	4.1	2.6	3.0	1.7	4.3	2.6	3.4	1.8	3.5	2.1	3.1	1.5
Li2019 shoot [85]	2.9	2.1	1.6	2.2	3.1	2.2	1.6	2.5	2.2	1.7	1.3	2.0
Li2019 root [84]	1.1	1.7	1.4	1.9	1.1	1.8	1.6	2.0	1.1	1.2	1.1	1.4
Li2019 leaf [84]	1.1	1.2	1.5	.9	1.3	1.6	1.8	1.0	1.0	1.1	1.1	.9
Li2019 internode [77]	1.6	2.3	1.9	1.5	1.6	2.8	2.2	1.6	1.3	1.6	1.3	1.0
Li2019 endosperm [121]	1.1	2.2	1.7	1.6	1.2	2.3	1.9	1.6	1.5	2.1	1.7	1.1
Li2019 6 tissues [620]	2.6	2.4	1.5	1.5	5.5	4.7	2.3	2.3	4.8	4.2	1.9	1.9
Huang2018 seed [159]	1.8	1.9	1.4	1.4	1.9	2.3	1.7	1.6	1.5	1.4	1.2	1.1
Huang2018 SAM [406]	3.1	3.7	2.6	2.6	2.6	4.1	2.8	2.6	1.4	3.0	1.9	1.6
Huang2018 root [176]	1.5	1.7	1.4	1.5	1.6	2.2	1.5	1.8	1.6	1.6	1.1	1.1
Huang2018 leaf [394]	1.8	2.0	1.4	1.1	2.8	3.0	2.9	1.8	1.7	1.9	1.8	1.5
Huang2018 4 tissues [1136]	6.8	5.1	2.0	2.8	7.8	5.9	2.5	3.0	6.2	4.2	1.7	2.8
Kremling2018 LMAN [249]	1.5	1.3	1.5	1.2	1.4	1.3	1.5	1.0	1.5	1.5	1.7	.7
Kremling2018 LMAD [199]	1.6	1.6	1.2	1.6	1.8	1.6	1.3	1.4	1.7	1.3	1.1	1.0
Kremling2018 L3Tip [257]	2.7	2.3	1.7	1.8	2.5	2.2	1.7	1.6	2.6	2.2	1.5	1.1
Kremling2018 L3Base [254]	1.4	1.7	1.2	1.2	1.7	2.0	1.3	1.3	1.5	2.2	1.4	.9
Kremling2018 Kern [226]	1.0	1.5	1.2	1.2	1.1	1.7	1.3	1.2	1.0	1.8	1.2	.8
Kremling2018 GShoot [271]	3.5	3.4	1.8	2.0	3.9	3.7	1.9	2.1	4.9	4.1	1.8	1.5
Kremling2018 GRoot [201]	1.7	2.6	1.6	1.6	1.5	2.5	1.6	1.5	1.2	2.2	1.5	1.1
Kremling2018 7 tissues [1657]	2.7	2.7	1.6	1.8	2.3	2.5	1.5	1.6	1.9	2.0	1.4	1.4
Lin2017 SAM [27]	1.4	3.4	2.6	1.4	1.5	3.4	2.0	1.4	1.4	3.4	1.8	1.0
Lin2017 tassel [26]	1.9	1.6	1.3	1.6	1.8	1.5	1.1	1.8	1.5	1.3	1.2	1.5
Lin2017 shoot [27]	4.7	4.2	2.1	1.9	10.8	9.4	3.4	2.7	2.7	2.7	1.6	1.8
Lin2017 root [27]	1.1	2.3	1.6	1.5	1.4	2.1	1.7	1.9	1.1	1.7	1.6	1.5
Lin2017 ear [26]	1.3	2.9	1.7	1.9	1.6	2.7	1.8	2.0	1.2	2.0	1.3	1.3
Lin2017 5 tissues [133]	3.7	3.5	2.0	2.0	3.5	3.8	2.2	2.4	1.5	2.7	1.8	1.9
Mazaheri2019 seedling [453]	1.4	1.1	1.2	1.4	1.9	1.6	1.3	1.6	1.3	1.1	1.0	.9
Shaefer2018 root_GCN [48]	1.7	5.7	3.4	3.0	1.8	6.0	3.5	2.9	1.4	7.6	3.9	2.0
Leiboff2015 SAM [383]	3.1	3.5	2.6	2.4	2.7	3.6	2.8	2.4	1.6	2.6	1.8	1.6
Hirsch2014 seedling [503]	1.5	1.3	1.2	1.5	1.6	1.5	1.3	1.5	.7	1.0	1.2	1.0
Fu2013 kernel [368]	1.5	2.0	1.4	1.6	1.4	2.3	1.5	1.7	1.3	1.7	1.3	1.2
Eichten2013 seedling_leaf3 [62]	3.9	3.4	1.7	2.1	4.2	3.7	1.8	2.2	5.2	4.2	1.8	1.9
Tissue Atlas combined [247]	8.2	7.0	2.9	2.9	9.2	8.1	3.3	3.3	6.2	5.2	2.2	2.3
Yi2019 seed dev [31]	1.3	1.5	1.2	1.3	1.2	2.4	1.7	1.3	1.0	.8	.9	1.1
Walley2016 B73 [23]	6.0	4.3	2.0	2.5	3.7	3.4	1.8	2.4	1.2	1.0	1.2	1.6
Stelpflug2016 B73 [93]	6.7	5.6	2.3	2.5	7.2	6.5	3.1	2.7	4.6	3.9	2.3	2.2

Fold Enrichment 2.5 5.0 7.5 10.0

Figure S2c. Comparison of GRNs built with different methods according to enrichment of functional annotations (Gene Ontology, CornCyc, etc).
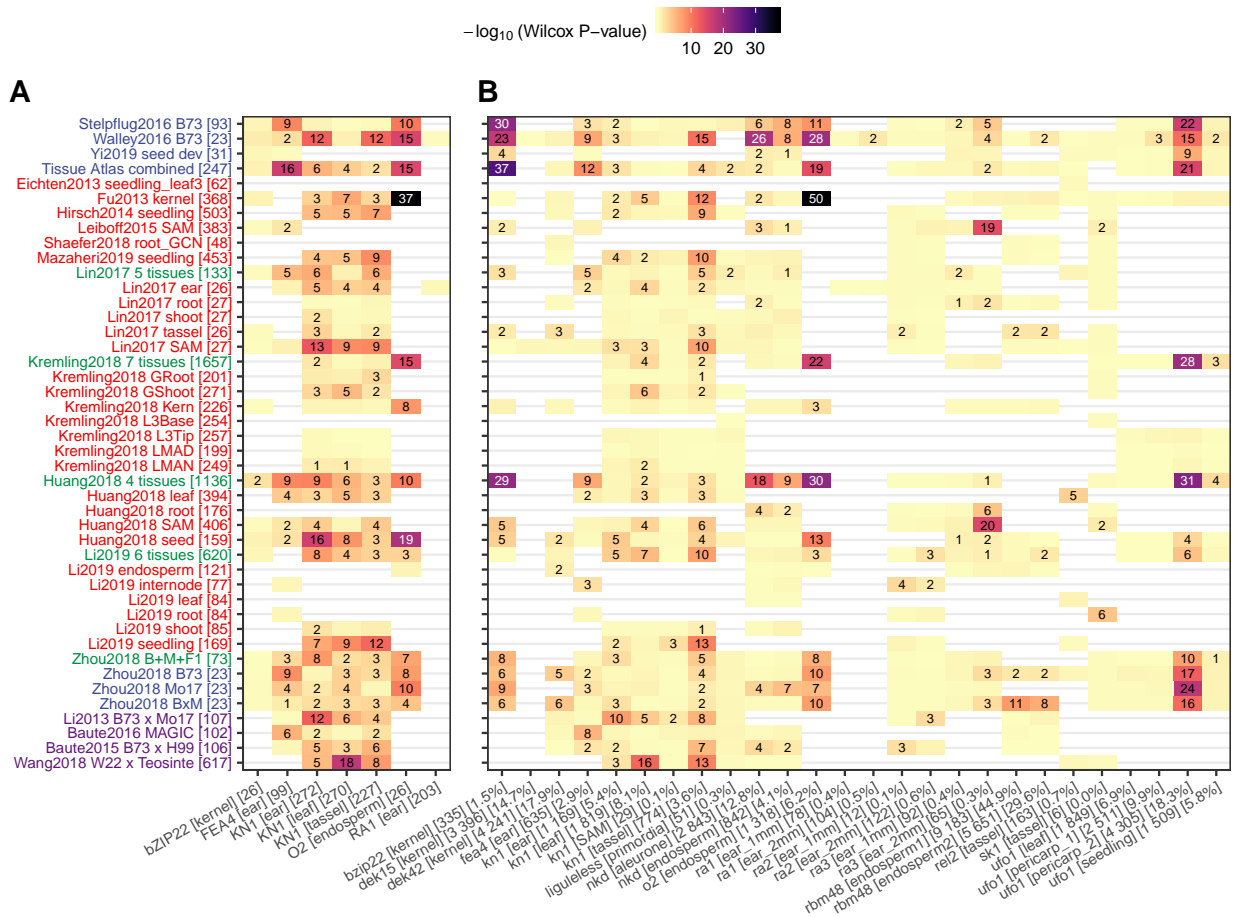
Figure 1. TF-target interactions predicted by GRNs are supported by knockout mutant RNA-Seq experiments. (A) direct targets of published TF studies; (B) For each one of the 21 maize TFs with knockout mutant RNA-Seq data available, differentially expressed genes between mutant and wildtype were identified using DESeq2 (p-value < 0.01). Wilcox rank test were then performed using the predicted (TF-target) interaction scores between the group of true targets (DEGs) and non-targets (non-DEGs). Numbers in each cell show the actual test P-value (-log10 transformed) with blank cells standing for "not significant" (P > 0.05). White cells stand for missing data where the TF being tested (knocked out) is not expressed in the corresponding GRN.
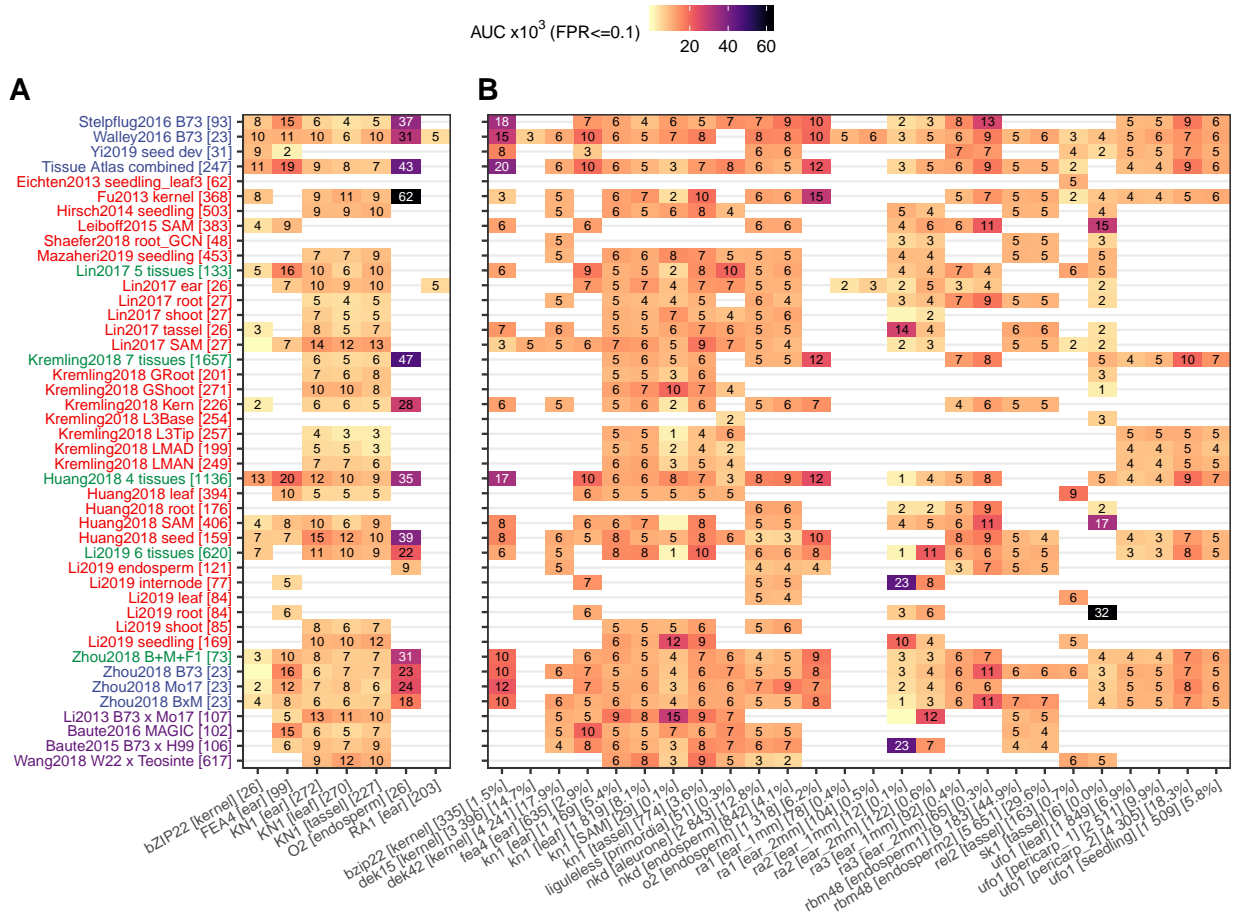
Figure S3. Area under receiver-operating characteristic curve (AUROC) evaluated for each GRN (until an False Positive Rate of 0.1 is reached) using support from (A) direct TF targets and (B) 21 maize TF knockout mutants as ground truth. Differentially expressed genes between each TF knockout mutant and the wildtype were identified using DESeq2 (p-value < 0.01) and treated as ground truth to evaluate GRN performance. Numbers in each cell show the actual AUROC values with white cells indicating missing data (the TF being filtered from the expression matrix due to invariable expression).
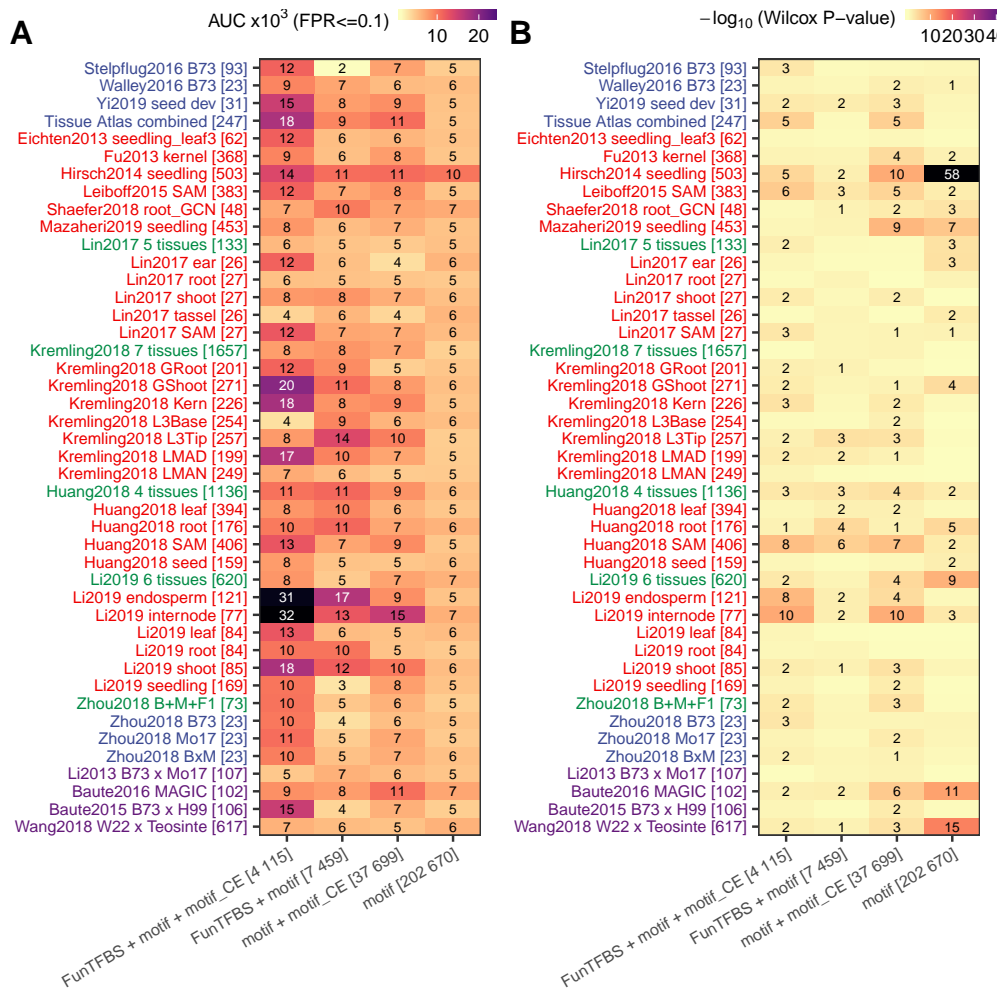
Figure S4. Evaluation (AUROC and Wilcox P-value) of constructed GRNs using four sets of predicted TF-target interactions based on TF-binding site motif, conserved element of TFBS motif or FunTFBS. There are 202,670 "motif"-based predictions, 37,699 predictions based on motif and cross-species conservation, 7,459 predictions based on motif and FunTFBS as well as 4,115 predictions based on all three evidences.
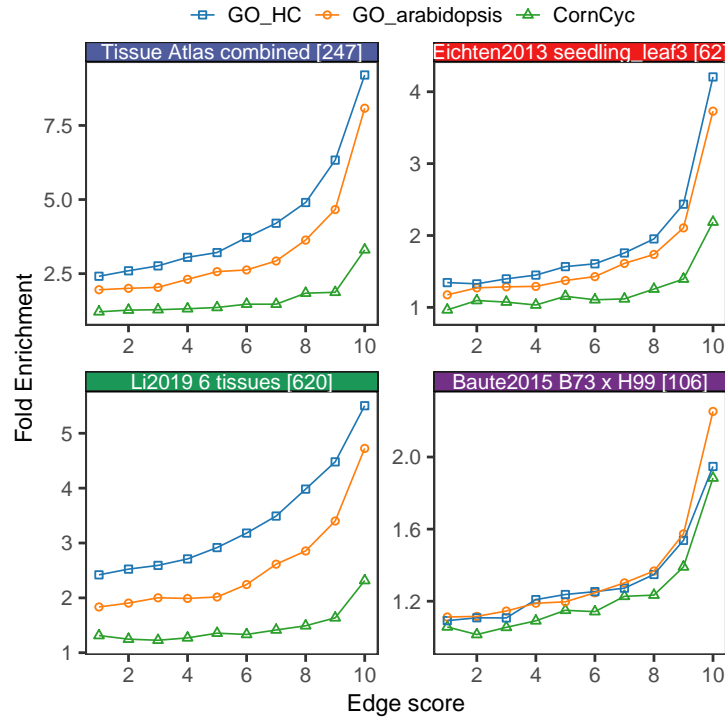
Figure 2. Enrichment of co-annotated GO/CornCyc terms in co-regulated network targets. For each network the top 1 million predicted TF-target associations were binned to 10 bins and assessed for enrichment of GO/CornCyc functional annotation. Fold enrichment is calculated as the observed number of shared GO/CornCyc terms (by targets regulated by a common TF) divided by the expected number of shared annotation terms (determined by permutation). The names for each of the networks are color coded to indicate B73 developmental surveys (blue), genotype surveys (red), meta-networks (green) or previously generated GRNs (teal).
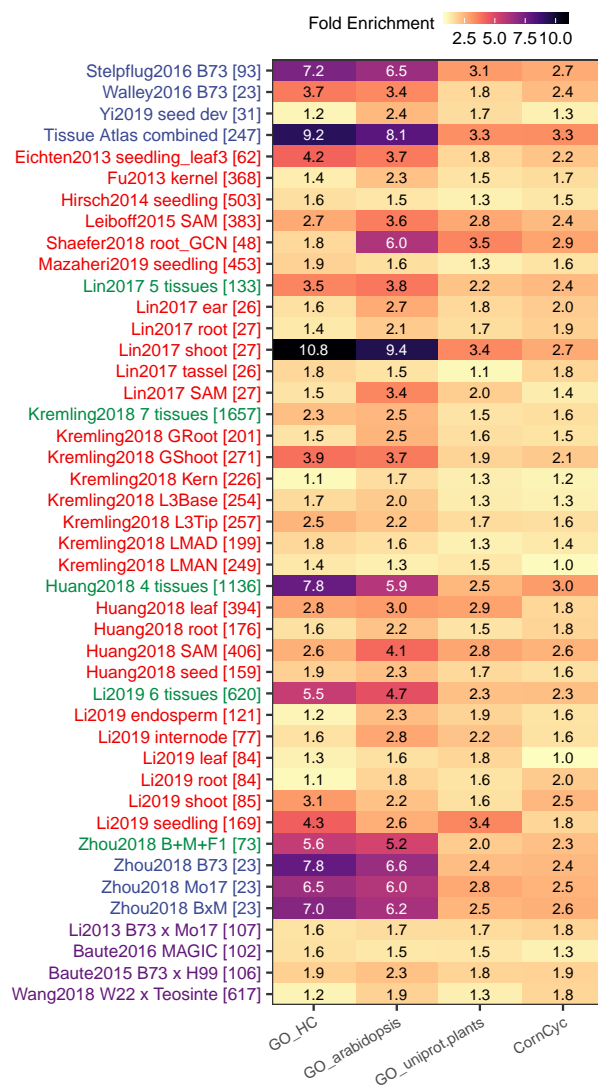
Figure 2b. Enrichment of co-annotated GO/CornCyc terms in co-regulated network targets. For each network the top 1 million predicted TF-target associations were binned to 10 bins and only the first bin (top 100k edges) were used to assess enrichment.
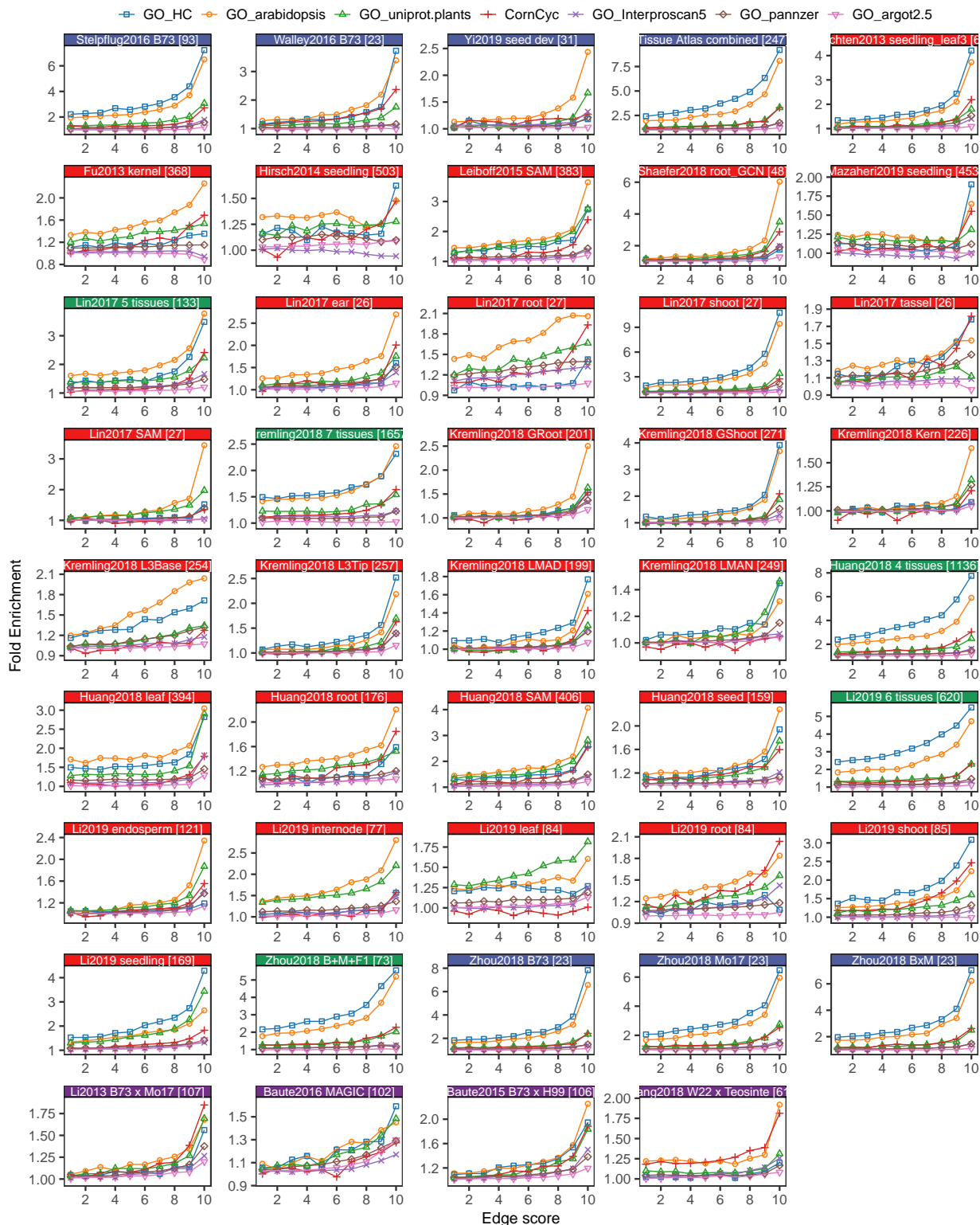
Figure S5. Enrichment of co-annotated GO/CornCyc terms in co-regulated network targets. For each network the top 1 million predicted TF-target associations were binned to 10 bins and assessed for enrichment of GO/CornCyc functional annotation. Fold enrichment is calculated as the observed number of shared GO/CornCyc terms (by targets regulated by a common TF) divided by the expected number of shared anno-

tation terms (determined by permutation). The names for each of the networks are color coded to indicate B73 developmental surveys (blue), genotype surveys (red), meta-networks (green) or previously generated GRNs (teal).

Figure 3. Hierarchical clustering of 44 GRNs. Pairwise distance between networks was determined by taking the top 100,000 TF-target predictions from each network and calculating the proportion of shared (common) predictions (using 'dist()' function in R with additional argument 'method=binary'). Hierarchical clustering was then performed based on the cross-network pairwise distance matrix using "ward.D" method.
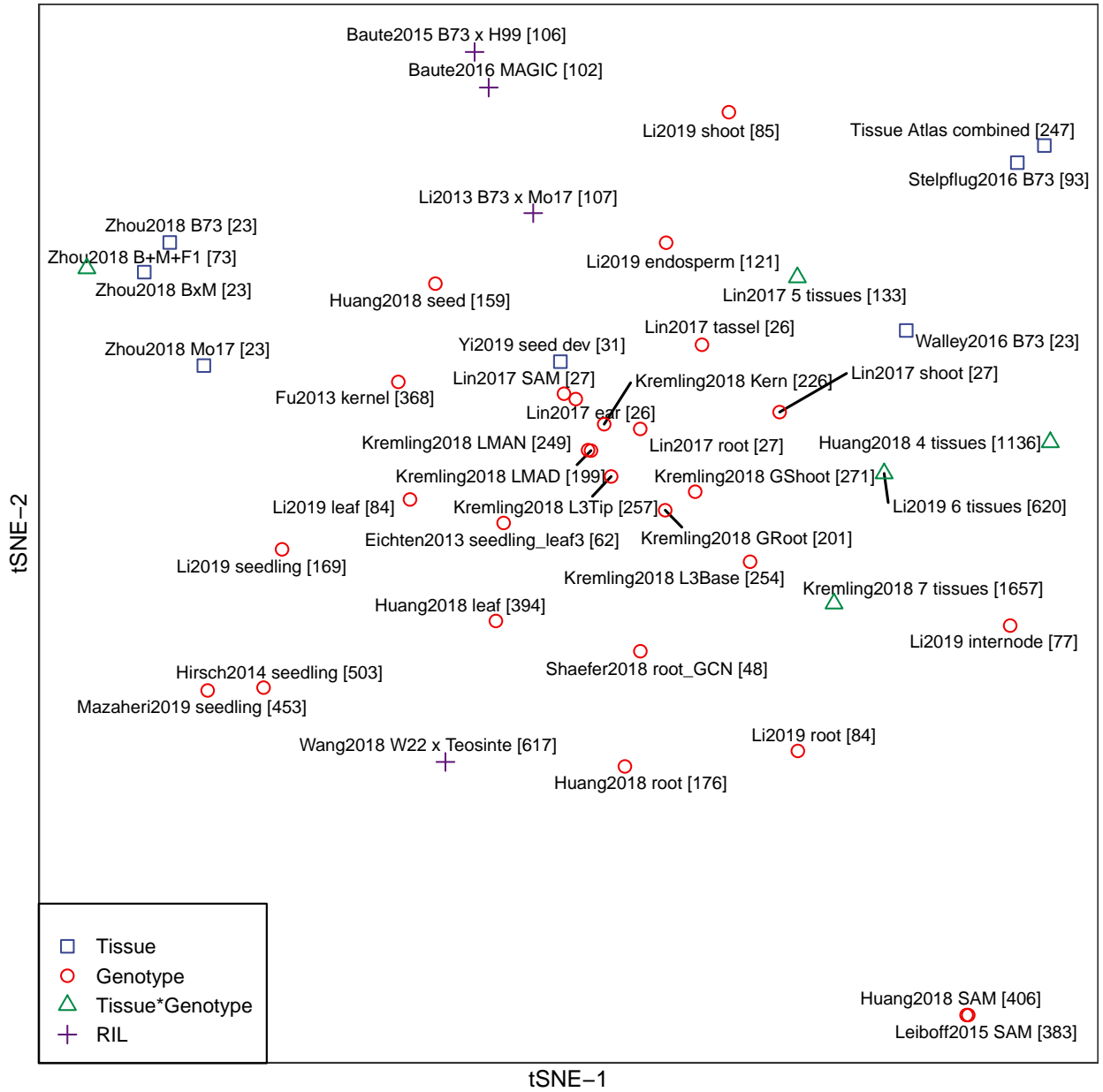
Figure S6. T-SNE clustering of 44 GRNs. Top 500,000 TF-target predictions were extracted from each network to perform t-SNE clustering using parameter "perplexing=9, permutation=2000".
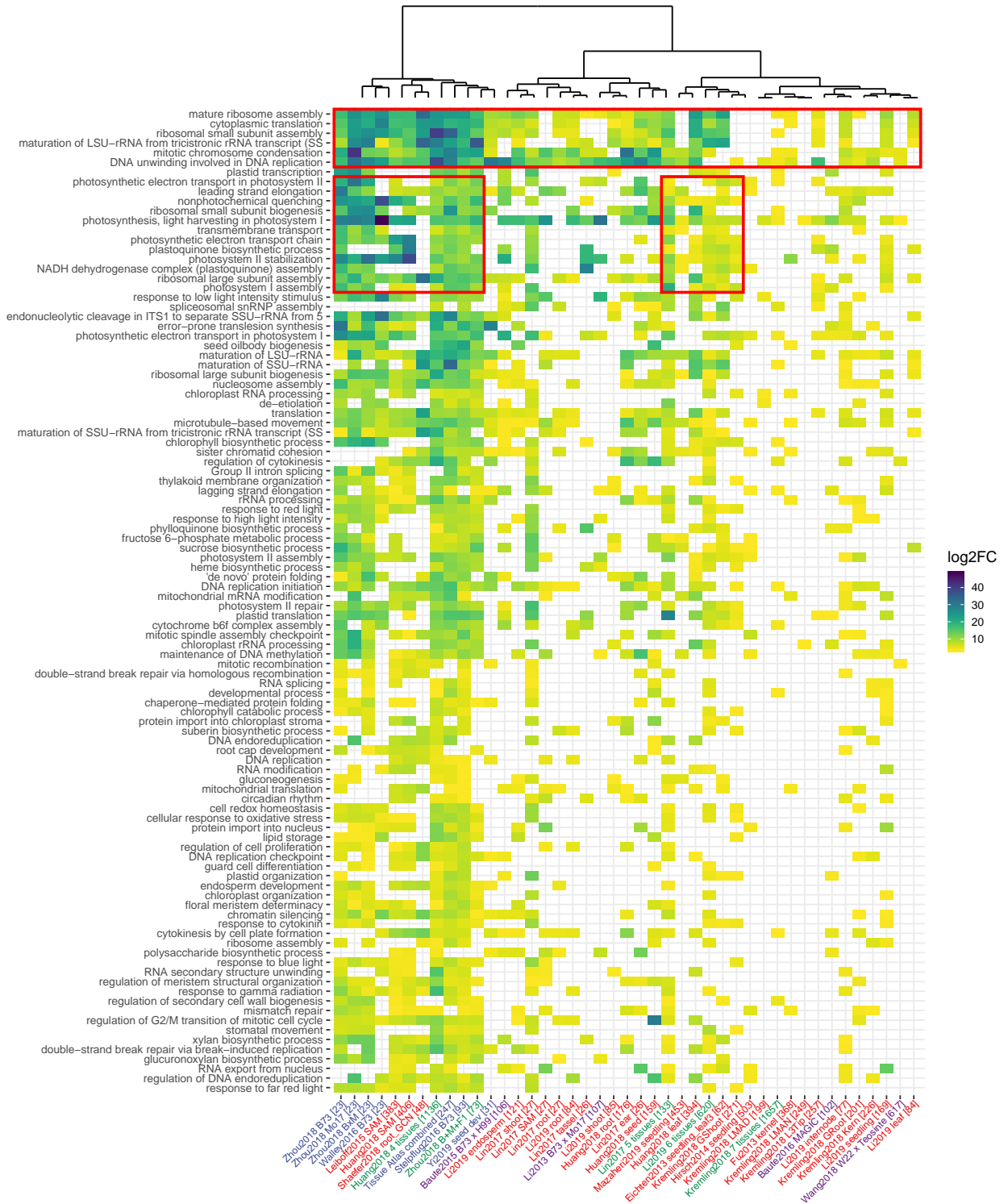
Figure 4. Hierarchical clustering of 140 Gene Ontology (Uniprot.Plants) terms using fold enrichment in different GRNs. Only GO terms enriched in at least 5 out of the 44 networks were used for clustering. Insignificant enrichment (p-value < 0.05) was treated as missing data and shown as white space in the figure.
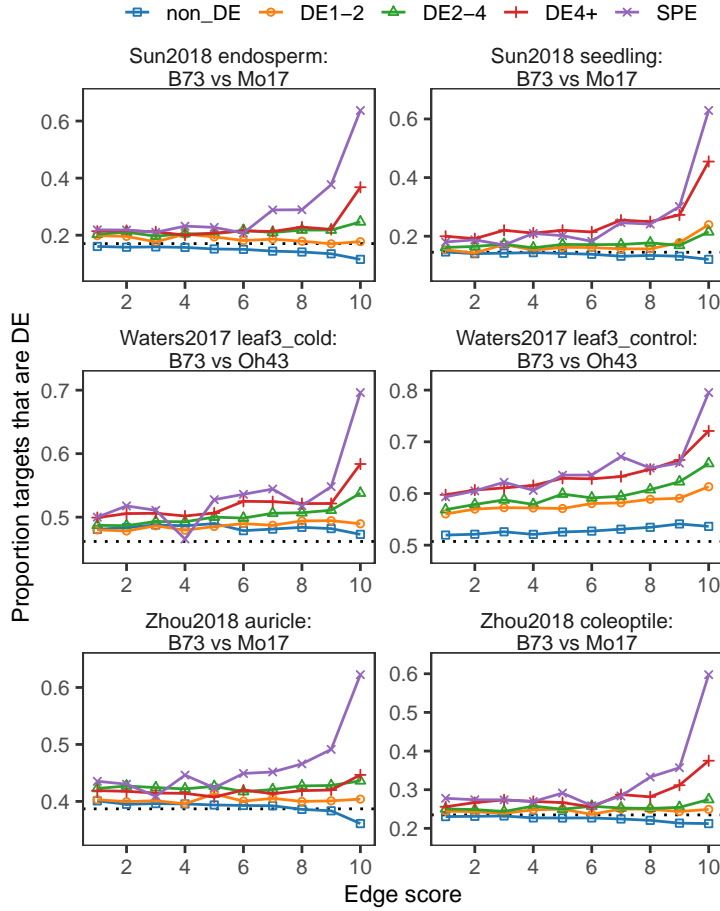
Figure 5. TF-target validation of the combined tissue network in three selected natural variation datasets. Each panel shows the proportion of differentially expressed targets regulated by TFs showing different DE levels between two genotypes in one tissue/treatment condition. For each network the top 1 million TF-target predictions were binned to 10 groups based on the interaction score in GRN. Each TF-target pair is classified according to the DE level of the TF ("non_DE", "DE1-2", "DE2-4", "DE4+" or "SPE") in each network. The proportion of TF-target pairs with the target also showing DE was then determined for each category. Dashed line in each panel represents the genome-wide (background) proportion of DE genes in each tissue/treatment setting.
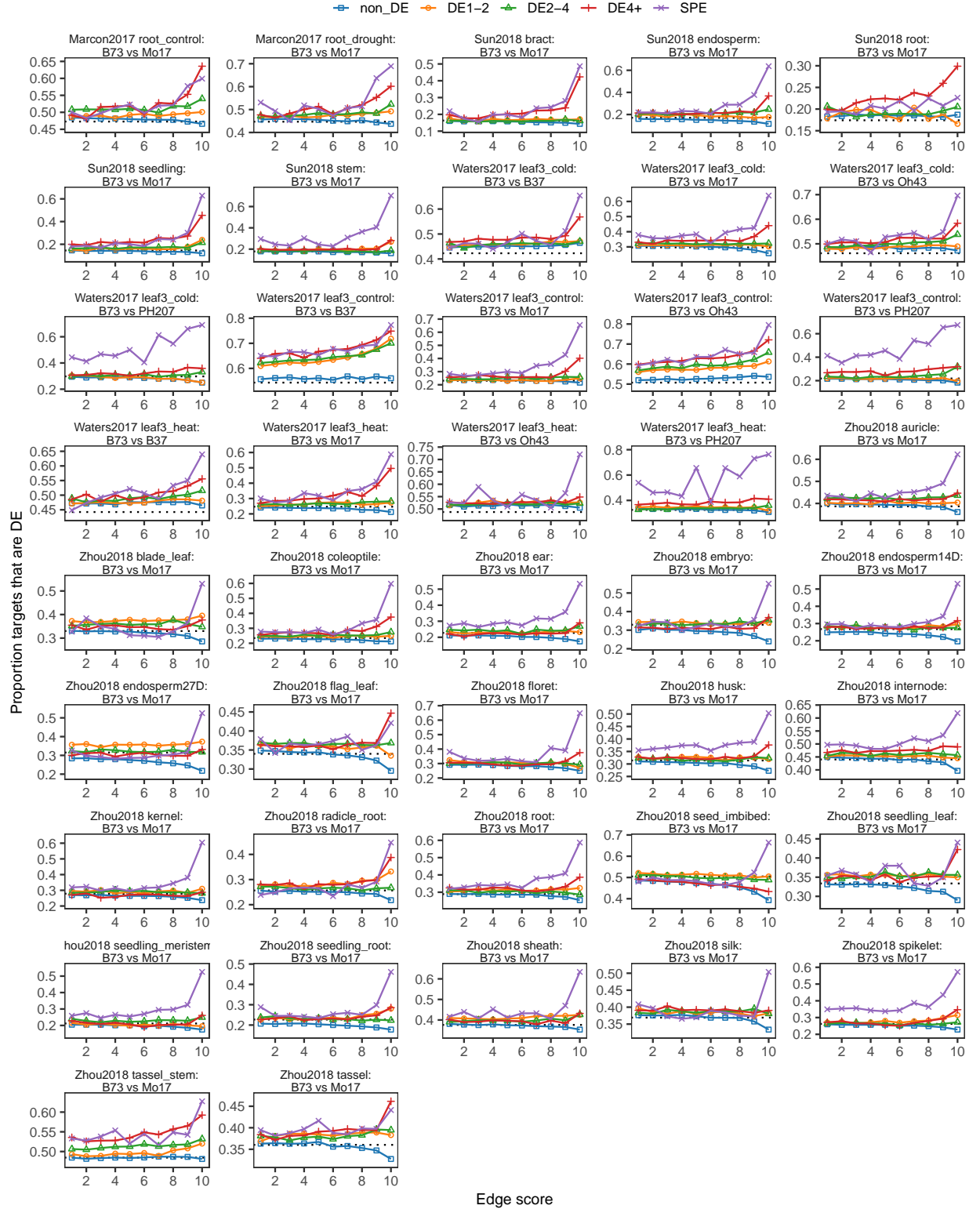
Figure S6. TF-target validation of the combined tissue network in all six selected natural variation datasets. Each panel shows the proportion of differentially expressed targets regulated by TFs showing different DE levels between two genotypes in one tissue/treatment condition. TF-target predictions were binned to 10 groups based on the interaction score in GRN. Each TF-target pair is classified according to the

DE level of the TF ("non_DE", "DE1-2", "DE2-4", "DE4+" or "SPE") in each network. The proportion of TF-target pairs with the target also showing DE was then determined for each category. Dashed line in each panel represents the genome-wide (background) proportion of DE genes in each tissue/treatment setting.
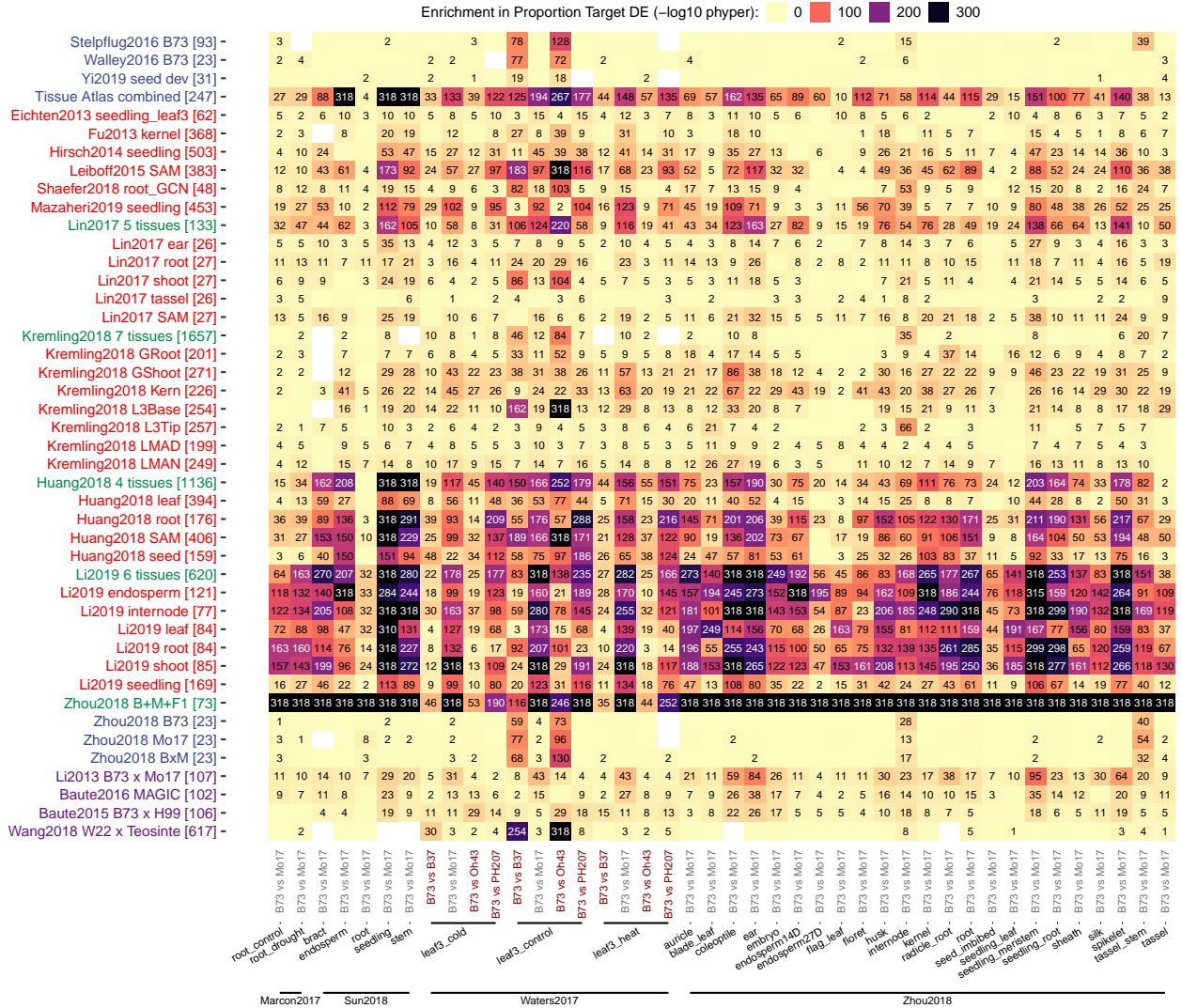
Figure 5b. Enrichment in differentially expressed targets regulated by TFs that show SPE patterns. Color and number in each cell represents the enrichment P-value (-log10 transformed, hypergeometric test p-value) of (SPE TF regulated) target DE proportions relative to the genome-wide proportion of DEGs for each GRN (row-wise) evaluated against a tissue/treatment condition in a natural variation dataset (column-wise). Only edges in the first bin (top 100k) of each network were taken.
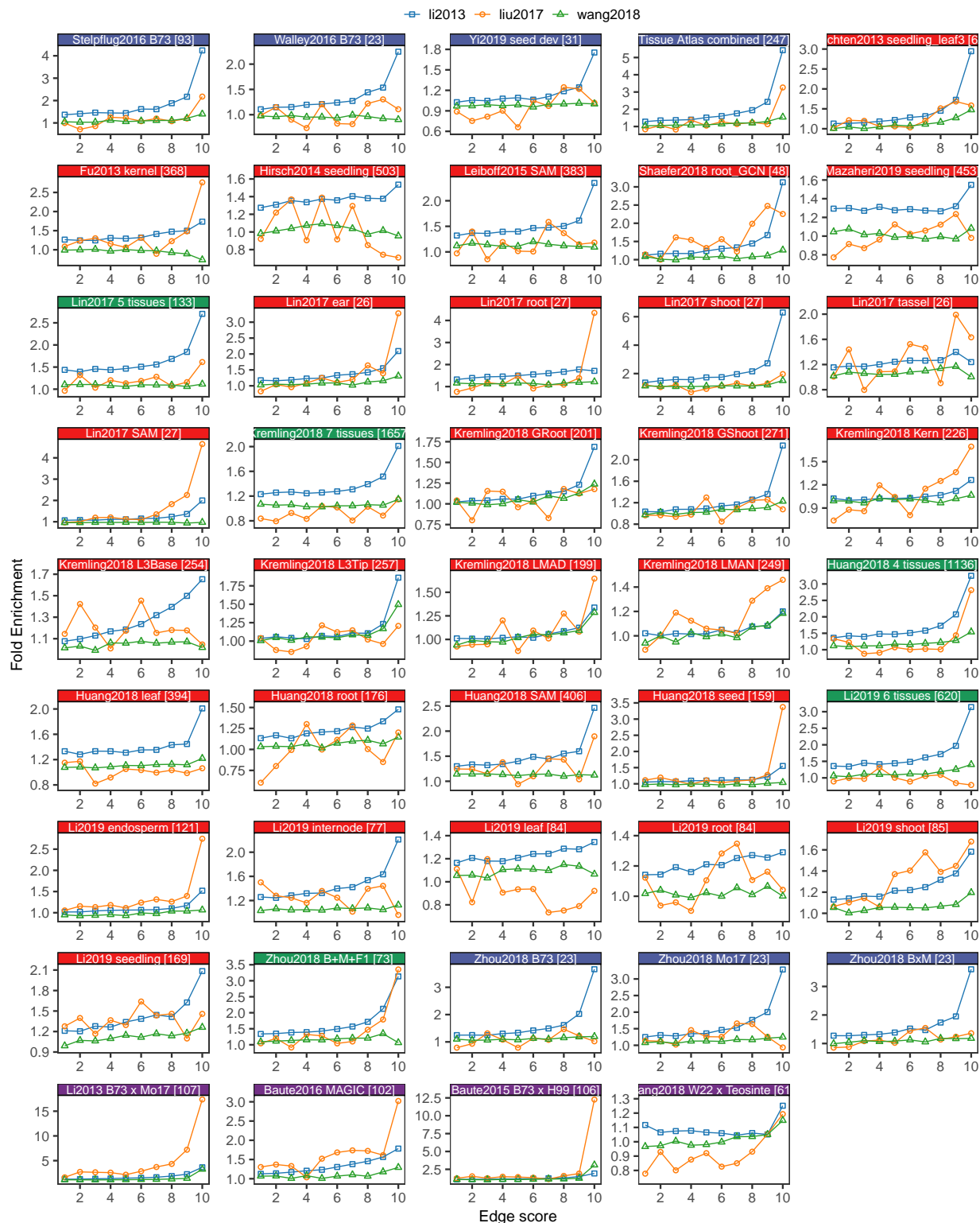
Figure S9. Enrichment of co-regulated targets between previously identified trans-eQTL hotspots and TF-target associations predicted by GRNs. For each network the top 1 million TF-target predictions were binned to 10 groups based on the interaction score in GRN. Fold enrichment is determined by the same permutation approach described in Figure 2.
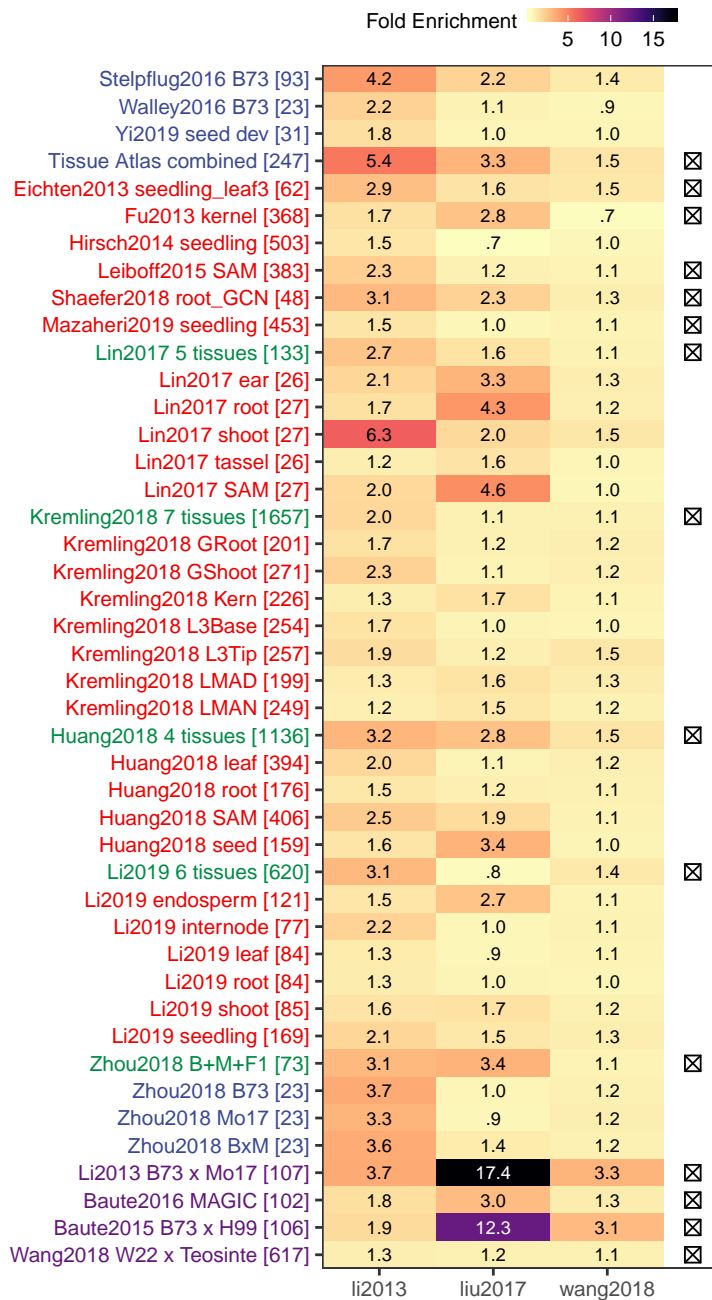
Figure S10. Enrichment of co-regulated targets between previously identified trans-eQTL hotspots and TF-target associations predicted by GRNs. For each network the top 1 million predicted TF-target associations were binned to 10 bins and only the first bin (top 100k edges) were used to assess enrichment. Fold enrichment is determined by the same permutation approach described in Figure 2.
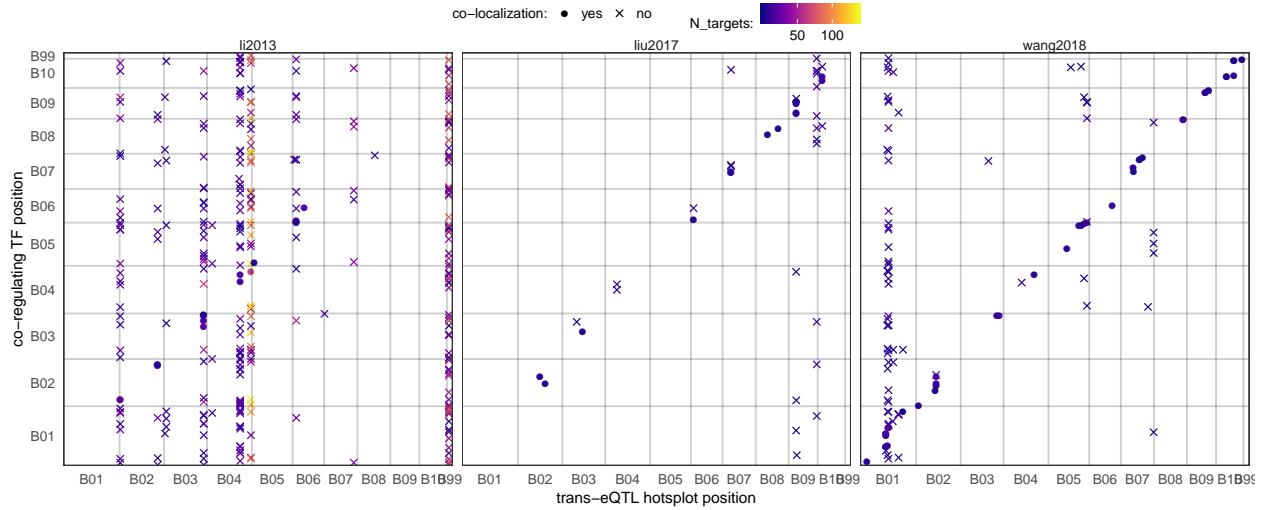
Figure S11. Co-localization of TFs predicted by GRNs in this study and trans-eQTL hotspots identified in previous studies that regulate the same set of targets. Each trans-eQTL hotspot were first tested for significant overlap in targets with any TFs (hypergeometric enrichment test as implemented in the phyper() function in R). To control for false positives, only TFs identified in at least two (out of 8 high quality networks, see Methods) that show significant co-regulation with at least one trans-eQTL hotspot (p < 0.01) were kept. Trans-eQTL hotspots identified in previous maize assemblies were lifted over to the AGPv4 assembly coordinates. Co-localization of a TF and a trans-eQTL is determined if the two coordinates are within 10-Mbp distance. Color of each dot represents the number of common targets between the predicted TF regulator and the trans-eQTL hotspot.
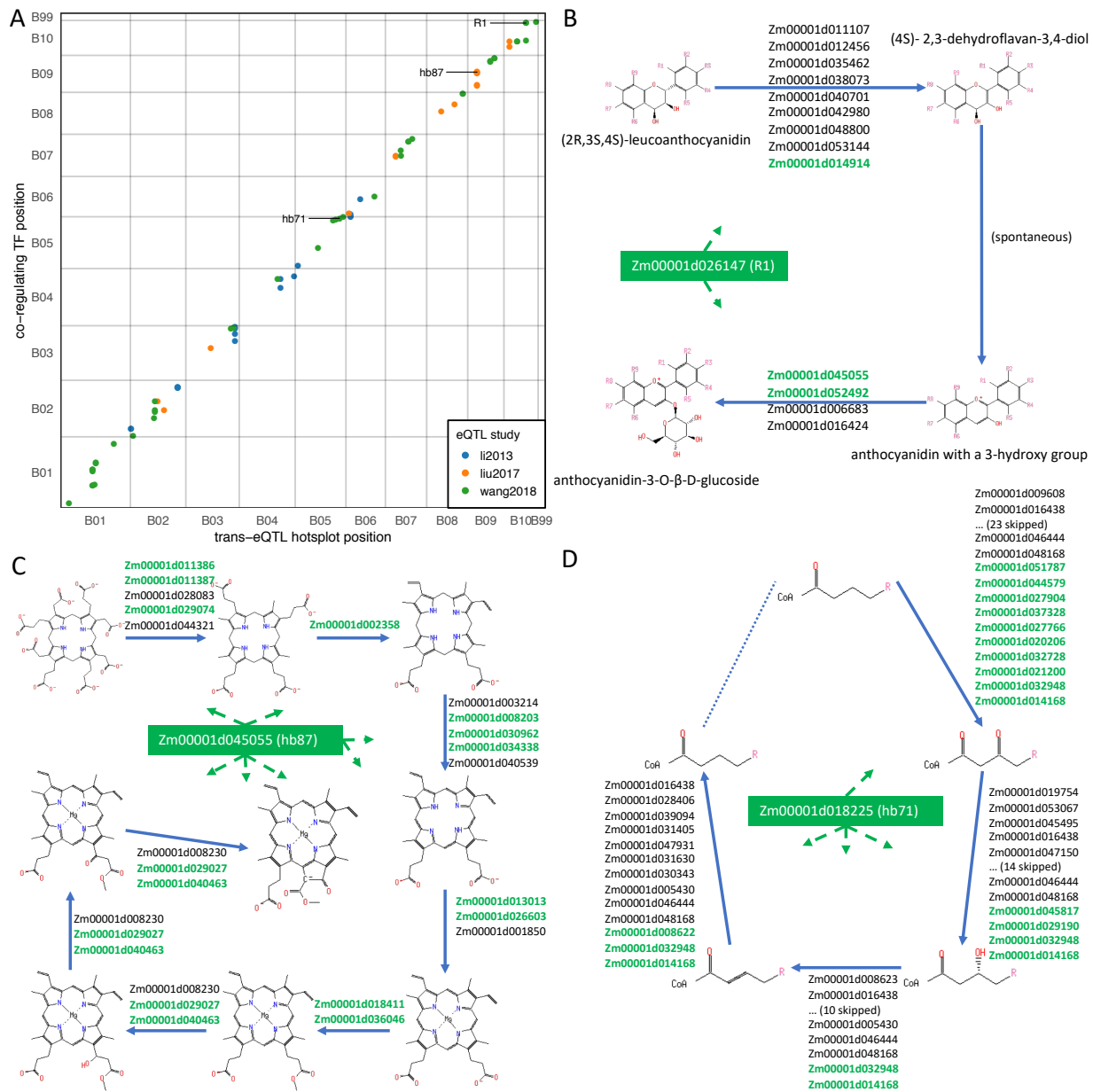
Figure 6. Identification of acting transcription factors underlying trans-eQTL hotspots identified in previous studies. (A) Co-localization of TFs predicted by GRNs in this study and trans-eQTL hotspots identified in previous studies that regulate the same set of targets. Each dot represents a TF supported by at least two high quality networks to show significant co-regulation with at least one trans-eQTL hotspot, and are within 10-Mbp distance from the trans-eQTL hotspot location; (B) Identification of R1 (colored, Zm00001d026147) co-localizing a previous trans-eQTL hotspot as the master regulator of the well studied anthocyanin biosynthesis pathway; (C) and (D) Identification of two previously uncharacterized TFs, the homeobox-transcription factor 87 (hb87, Zm00001d046405) and MYB-transcription factor 61 (myb61, Zm00001d053124) that co-localize previous trans-eQTL hotspots as the master regulator of the chlorophyllide biosynthesis pathway and the major CO2 fixation pathway (Calvin cycle pathway), respectively.